IEEE Photonics Journal
An IEEE Photonics Society Publication

Cross-Gain Modulation and Four-Wave Mixing for Wavelength Conversion in Undoped and p-Doped 1.3-μm Quantum Dot Semiconductor Optical Amplifiers

Volume 2, Number 2, April 2010

Christian Meuer
Holger Schmeckebier
Gerrit Fiol
Dejan Arsenijević
Jungho Kim, Member, IEEE
Gadi Eisenstein, Fellow, IEEE
Dieter Bimberg, Senior Member, IEEE

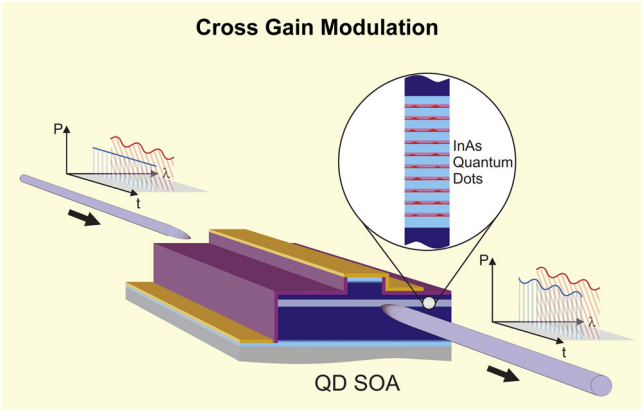

DOI: 10.1109/JPHOT.2010.2044568
1943-0655/$26.00 ©2010 IEEE

Cross-Gain Modulation and Four-Wave Mixing for Wavelength Conversion in Undoped and p-Doped 1.3-μm Quantum Dot Semiconductor Optical Amplifiers

Christian Meuer,[1] Holger Schmeckebier,[1] Gerrit Fiol,[1] Dejan Arsenijević,[1] Jungho Kim,[2] *Member, IEEE*, Gadi Eisenstein,[3] *Fellow, IEEE*, and Dieter Bimberg,[1] *Senior Member, IEEE*

[1]Institut für Festkörperphysik, Technische Universität Berlin, 10623 Berlin, Germany
[2]Department of Information Display, Kyung Hee University, Seoul 130-701, Korea
[3]Electrical Engineering Department, Technion–Israel Institute of Technology, Haifa 32000, Israel

DOI: 10.1109/JPHOT.2010.2044568

Manuscript received November 16, 2009. First published Online February 25, 2010. Current version published March 19, 2010. This work was supported by the Research Center SFB 787 of the German Research Foundation. The work of G. Eisenstein was supported by the Alexander von Humboldt Foundation. Corresponding author: C. Meuer (e-mail: chmeuer@sol.physik.tu-berlin.de).

Abstract: P-doped and undoped quantum dot (QD) semiconductor optical amplifiers (SOAs) having a similar chip gain of 22–24 dB are compared with regard to their static and dynamic characteristics. Amplified spontaneous emission (ASE) spectra reveal the influence of p-doping on the gain characteristics and the temperature stability. In contrast to QD lasers, p-doping does not significantly increase the thermal stability of QD SOAs. The static four-wave mixing efficiency is larger and more temperature stable in undoped devices, leading to a maximum chip conversion efficiency of -2 dB. Small-signal cross-gain modulation (XGM) experiments show an increase in the small-signal bandwidth from 25 GHz for the p-doped SOAs to 40 GHz for the undoped QD SOAs at the same current density. P-doped QD SOAs also achieve small-signal bandwidths beyond 40 GHz but at a larger bias. The XGM is found to be temperature stable in the range of 20 °C to 40 °C.

Index Terms: Semiconductor optical amplifiers, quantum dots, p-doping, cross-gain modulation, four-wave mixing.

1. Introduction

The strong demand for increasing communication network capacity is driving the rapid development of more powerful all-optical metropolitan area networks like the 100-Gb/s Ethernet. For these networks, ultrahigh-speed devices for linear amplification, as well as for nonlinear signal processing, are in high demand. Semiconductor optical amplifiers (SOAs) are applicable for both linear amplification as well as signal processing and feature a small footprint and low cost in mass production. Signal processing includes wavelength converters, switches, and regenerators and is enabled by nonlinear effects occurring when the amplifier is driven in saturation. The nonlinear effects we are focusing on in this paper are cross-gain modulation (XGM) and four-wave mixing (FWM) for wavelength conversion.

SOAs based on a quantum dot (QD) gain material are superior to conventional bulk or quantum well (QW) devices [1]–[3]. Their main advantages are the size distribution of the QDs, resulting in a wide gain spectrum [4], the ultrafast dynamics within the QDs [5] enabling high-speed operation at 40 Gb/s or more [6]–[8], and high saturation output powers [9]. Both calculations and recent pump-probe experiments indeed predict operation at data rates above 100 Gb/s [6], [10].

P-doping of the QD active region was supposed to increase the temperature stability of the threshold current density [11] and the high-speed characteristics of QD lasers [12], [13]. However, in pump-probe measurements on QD SOAs, slower gain recovery dynamics was found [14], [15]. We will compare here the static as well as the dynamic characteristics of otherwise identical real QD SOAs which are doped or undoped to judge the influence of p-doping on the amplifier performance. We will focus in particular on the nonlinearities enabling wavelength conversion, i.e., XGM and FWM and their temperature dependence.

This paper is organized as follows. A short description of the QD material and the device layout is given in Section 2. The static comparison between p-doped and undoped QD SOAs is presented in Section 3. Subsequently, FWM and small-signal XGM measurements are shown in Sections 4 and 5, respectively, followed by a conclusion in Section 6.

2. Epitaxy and Device Structure

The p-doped as well as the undoped QD SOAs were processed from material grown by molecular beam epitaxy and contain ten stacks of InGaAs/GaAs QDs. In order to shift the emission to 1.3 μm, each dot layer is overgrown with an InGaAs-QW (dots in a well structure). Barrier layers that are 33 nm thick provide strain relaxation between the QD layers. In the case of the p-doped QD SOAs, a 10-nm-thick part of the spacer layer which is 9 nm below the QD layer is p-doped $(5 * 10^{17}\ \mathrm{cm}^{-3})$. This leads to a prefilling of the QD hole states. The stacked QDs were incorporated in an AlGaAs/GaAs-based laser structure. A dry etching process was used to form shallow etched ridges which are 4 μm in width. The SOAs are antireflection $(R < 10^{-3})$ coated and tilted at an angle of 8° in order to suppress the onset of lasing at higher current densities. The remaining gain ripple is below 0.3 dB for all devices shown here. Due to some fluctuations in the growth process the peak emission of the undoped samples is at 1290 nm, whereas the p-doped SOAs have a peak gain at 1310 nm.

The electronic structure of a QD embedded in a QW comprises a ground state (GS) which is used for amplification and a carrier reservoir in higher energy states, i.e., the excited states (ESs) and the QW. The ES enables ultrafast recovery of the GS population [5], whereas the recovery of the QW population after saturation seems to be rather slow [16], leading to a second slower refilling time constant of the QDs. From this unique electronic structure, two different saturation mechanisms arise. The total carrier depletion by exhaustion of the carrier reservoir in the higher energy states leads to dynamics on a 100-ps time scale. In addition, spectral hole burning occurs, if only the GS is depleted, but the carrier reservoir remains highly populated. The recovery of spectral hole burning takes place on a subpicosecond time scale enabling high-frequency operation. Thus, the devices show faster dynamics at large current densities [8]. The maximum current which presently can be applied is limited by mounting dependent thermal heating of the device, which leads to a red shift of the spectrum and a corresponding decrease of the linear gain.

3. Comparison of Static Properties

A basic comparison reveals that p-doping increases the linear gain per length by almost 50%. The values for the devices measured here are 10 dB/mm and 7 dB/mm for p-doped and undoped QD SOAs, respectively. Since the gain directly influences the dynamics by determining the number of carriers which are depleted at a given input power level and the degree of saturation in which the amplifier is driven, devices with equal chip gain are mandatory for a correct comparison.

In [14], the chip gain was tuned via the injection current for devices having the same physical length. Hence, the p-doped samples having a larger gain were driven at less injection current. However, in [8], it has been demonstrated that the QD SOA frequency bandwidth is strongly increased at large injection currents. The linear gain reaches its maximum due to complete inversion of the GS and the reservoir is sufficiently populated in order to enable fast recovery of the GS gain. Therefore, we compare devices having the same linear gain but different lengths which can be compared at equal injection current densities.

Therefore, 2-mm-long p-doped and 3-mm-long undoped devices were fabricated having nearly the same fiber-to-fiber gain of 13 dB and 14.5 dB, respectively, corresponding to 22 dB and 23.5 dB chip gain, respectively. As a result of the length difference the fiber-to-fiber noise figure of 10 dB of

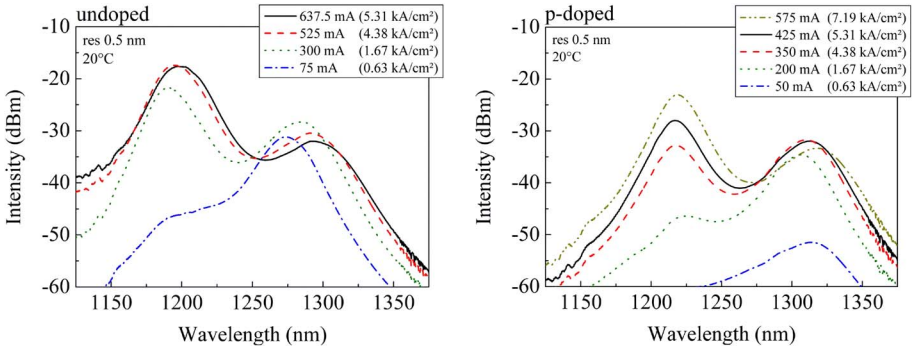

Fig. 1. (Left) Spectra of the ASE of the undoped 3-mm-long QD SOA in dependence on the bias current at 20 °C showing a maximum GS luminescence between 187.5 mA and 300 mA. At larger currents, a red shift due to heating is observed. The ES luminescence reaches saturation at 525 mA. The spectral resolution is set to 0.5 nm. (Right) Spectra of the ASE of the p-doped 2-mm-long QD SOA in dependence on the bias current at 20 °C showing a maximum GS luminescence at 350 mA. At larger currents heating induces a red shift. The ES state luminescence does not saturate up to 575 mA.

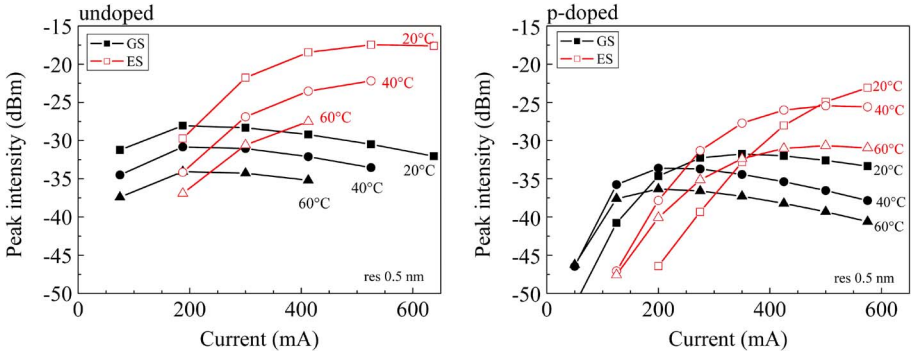

Fig. 2. (Left) Peak intensity of the GS (black, filled symbols) and ES (red, open symbols) luminescence for undoped QD SOAs is shown and is dependent on the operating current at temperature of 20 °C, 40 °C, and 60 °C. The GS luminescence saturates at 200 mA and decreases for larger currents. The ES saturates at 500 mA. At elevated temperatures, the intensity decreases linearly (in a decibel scale) at a given current. (Right) Peak intensity of the GS (black, filled symbols) and ES (red, open symbols) luminescence for p-doped QD SOAs is shown and is dependent on the operating current at temperature of 20 °C, 40 °C, and 60 °C. At higher temperature, a larger emission is observed at lower injection current. However, the maximum peak intensity decreases by 3 dB per 20 °C increment comparable to the undoped QD SOAs.

the undoped QD SOAs is 1 dB larger than for the p-doped ones. Furthermore, the saturation output power in fiber of the undoped SOAs is larger (up to 15 dBm compared with 12 dBm). The corresponding spectra of the amplified spontaneous emission (ASE) of the undoped and p-doped QD SOAs are shown in Fig. 1. The colors represent same current densities at which the spectra were recorded for both devices. The undoped samples have a larger GS emission at smaller current densities and reach a maximum at approximately 200 mA. For currents above 300 mA, the GS experiences a red shift, and the intensity decreases due to thermal heating. On the other hand, the luminescence of the p-doped QD SOAs reaches its maximum beyond 350 mA, which corresponds to an almost doubled current density as compared with undoped SOAs. The ES emission of the undoped amplifiers at 1200 nm is more intense, whereas the p-doped devices show, even at the maximum current, no saturation of the ES. The luminescence is still 5 dB lower in intensity than for the undoped material. The results are consistent with the results shown in [14].

The temperature dependent evaluation of the ASE spectra shows a completely different behavior of the undoped and p-doped samples. ASE spectra similar to the ones shown in Fig. 1 were measured for various currents at temperatures of 20 °C, 40 °C, and 60 °C, and the intensity of the GS and ES peaks are plotted in Fig. 2.

The undoped QD SOAs show a saturation of the GS ASE intensity near 200 mA independent of the temperature. At elevated temperatures of 40 °C and 60 °C, the intensity decreases by 3 dB, while the trend of the current dependence is preserved. The ES decreases by 5 dB and 3 dB, respectively, upon increasing the temperature from 20 °C to 40 °C and from 40 °C to 60 °C, respectively. The trend upon an increase of current remains the same.

The p-doped samples reach the maximum luminescence of the GS at 350 mA at 20 °C, and the ES is even at very large currents is not saturated, as stated above. If the temperature is increased the maximum intensity decreases similar to the undoped samples. However, the maximum intensity is reached at a current of 200 mA between 40 °C and 60 °C, resulting in a shift of the curve to lower currents. Additionally, the ES saturates at elevated temperatures.

These findings demonstrate that p-doping has two different major influences on the device parameters.

First, p-doping provides excess holes which populate the QD hole states, whose energy separation is much smaller than for the electron states due to the larger effective mass. This ensures that the inversion is not reduced by thermal smearing of the hole population across the hole states. Thus, in p-doped devices the hole inversion is larger and, in turn, the gain is increased, as originally proposed for QD lasers [17].

Second, p-doping gives rise to some nonradiative recombination (NRR), as discussed in [18]. NRR consumes a significant amount of the injected carriers and leads to the observed behavior of the gain which reaches its maximum at much larger current densities than for undoped devices.

Additionally, the carrier population in the reservoir in the ESs is smaller, because the carriers in the GSs are depleted faster due to the larger gain. Thus, the recovery of the QD GS population is limited by the depletion of the reservoir and the scattering into the QDs rather than by intradot relaxation from ES to GS [19], resulting in a stronger coupling to the reservoir dynamics. On the other hand, in undoped devices, the reservoir is highly populated and less saturated. This enables larger saturation output power levels and, in particular, faster dynamics of QD SOAs [8], [20], [21]. In contrast with that, QD lasers are operated at lower current densities, and their modulation bandwidth benefits from the larger differential gain in p-doped devices.

At larger temperatures, the behavior of the p-doped QD SOAs changes significantly. As seen in Fig. 2 the gain is increased at lower injection current levels if the temperature is raised from 20 °C to 40 °C. This phenomenon is well known from QD lasers and leads to a decreasing threshold current density with increasing temperature [11] and is attributed to a reduced NRR at elevated temperatures. This allows for QD lasers with superior temperature stability. However, for QD SOAs, it is more important to achieve a temperature independent maximum GS gain. As shown in Fig. 2, the GS gain decreases for both sample types by 3 dB per 20 °C temperature increase. The according wavelength shift of the gain spectrum is similar. Therefore, the gain of undoped and p-doped QD SOAs has a quite comparable trend, if the temperature changes and p-doping does not improve the temperature stability of the peak gain of QD SOAs, which is in undoped and p-doped devices determined by the inversion of the QD states. Due to larger escape rates from the QDs into the surrounding QW the gain decreases at high temperature. These observations lead to the conclusion that independent of the doping, the carrier escape rate is the crucial parameter influencing the inversion and, hence, the gain at elevated temperatures.

Thus, in contrast to QD lasers p-doping does not increase the temperature stability of QD SOAs. Due to the larger gain and NRR, the reservoir is less populated at similar current densities, which is detrimental for high-speed operation in deep saturation. P-doped QD SOAs, however, are advantageous for linear signal amplification due to the larger gain per length, enabling shorter devices with lower waveguide losses and a reduced noise figure.

4. Four-Wave Mixing

The investigation of FWM is focusing on static characteristics in this paper. Previous measurements by us on similar samples [22] and investigations of 1.55-μm InP-based [23] QD SOAs

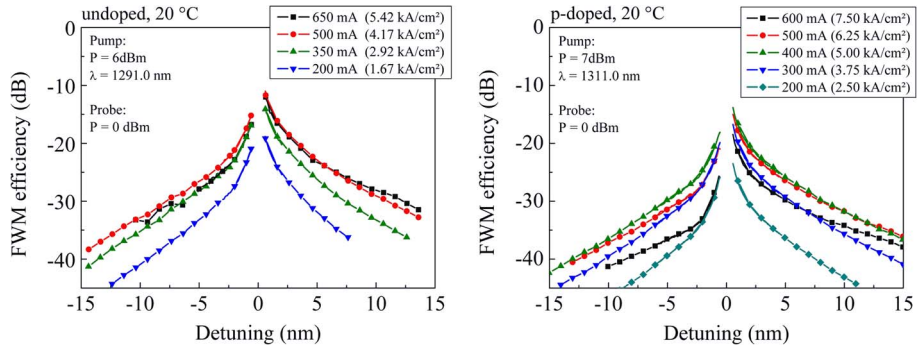

Fig. 3. (Left) FWM efficiency of the undoped QD SOAs at 20 °C dependent on the detuning shown for various currents. The maximum fiber-to-fiber efficiency is −11 dB, which corresponds to a chip efficiency of −2 dB at a detuning of 0.61 nm. (Right) FWM efficiency of the p-doped QD SOAs at 20 °C dependent on the detuning shown for various currents. The maximum fiber-to-fiber efficiency is −14 dB and thus 3 dB lower than in the undoped devices. Even current densities larger than for the undoped SOAs enable no improved FWM efficiency.

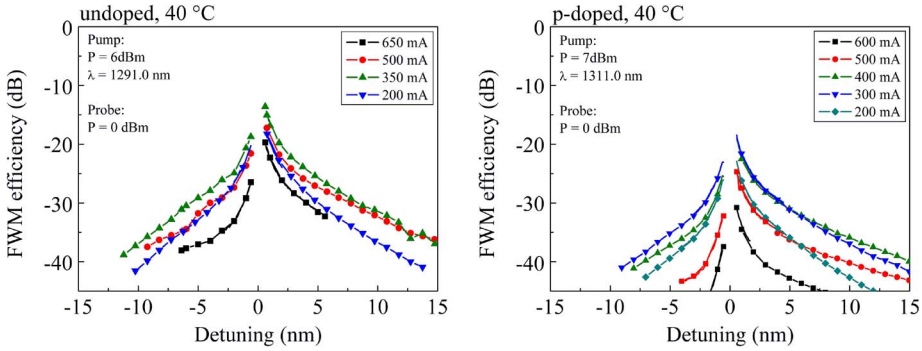

Fig. 4. (Left) FWM efficiency of the undoped QD SOAs at 40 °C dependent on the detuning shown for various currents. The efficiency remains almost constant at 350 mA. At larger currents, the efficiency is decreased, and the asymmetry becomes higher. (Right) FWM efficiency of the p-doped QD SOAs at 40 °C dependent on the detuning shown for various currents. The optimum efficiency decreases by 4.5 dB, and a stronger asymmetry emerges.

have already shown bandwidths well exceeding the range up to 40 GHz that is accessible with our lab equipment. For FWM the conversion efficiency, however, is the decisive figure of merit rather than the modulation bandwidth. Wavelength conversion via FWM is usually limited by low conversion efficiency and the accompanying deterioration of the signal-to-noise ratio. Additionally, the wavelength span for conversion is only in the range of a few nanometers around the pump wavelength.

In static measurements two saturating signals, called pump and probe, are injected. The pump signal has a fixed wavelength, whereas the wavelength of the probe is tuned to measure the FWM conversion wavelength range at various drive currents. The FWM efficiency is defined as the ratio of the power of the output FWM signal to the input probe signal. It is plotted on a semilogarithmic scale in Figs. 3 and 4. The detuning determines the wavelength difference of the probe wavelength to the pump wavelength. The FWM conjugate is generated at inverse detuning.

The results at 20 °C are shown in Fig. 3 for the undoped and p-doped samples, respectively. For undoped devices, a maximum conversion efficiency of −11 dB at a detuning of 0.6 nm is achieved. A fiber-to-fiber conversion efficiency of −11 dB corresponds to a chip efficiency of −2 dB if the coupling losses are considered. The efficiency increases at an even lower detuning which, however, is not experimentally accessible. This result is comparable with values found in the literature [24], [25]. The FWM efficiency is 3 dB smaller for the p-doped QD SOAs at comparable current densities across the

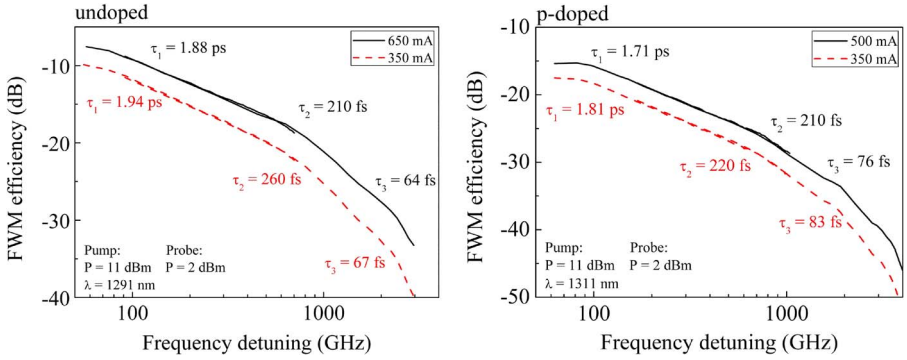

Fig. 5. (Left) FWM efficiency of undoped QD SOAs plotted versus the frequency detuning. From characteristic points, time constants are deduced, as shown in the figure. These correspond presumably to the scattering into the QDs (τ_1), the intradot relaxation from ES to GS for electrons and for holes (τ_2 and τ_3, respectively). (Right) FWM efficiency of p-doped QD SOAs plotted versus the frequency detuning. From characteristic points, time constants are deduced, as shown in the figure.

entire conversion range. The efficiency is not increasing, even if the p-doped QD SOAs are biased at much larger current densities.

This FWM efficiency decrease is caused by the stronger coupling to the reservoir in p-doped devices, because the reservoir is less populated and stronger depleted due to the larger gain. Thus, the slow recovery of the reservoir limits QDs dynamics. As a result, the contribution of the spectral hole as compared to carrier heating and carrier density pulsation is smaller, and as a consequence, the dependence on the detuning shows a larger asymmetry.

If the temperature is increased to 40 °C (see Fig. 4), the efficiency remains almost constant up to 350 mA and 400 mA for the undoped and p-doped QD SOAs, respectively. However, it decreases at larger currents significantly due to heating and a more pronounced coupling of the QDs and reservoir states. This coupling results from increased carrier escape rates at elevated temperatures. Therefore, the maximum FWM efficiency achievable is 3 dB (undoped) and 4.5 dB (p-doped) smaller at 40 °C. From 40 °C to 60 °C, the FWM efficiency drops by another 14 dB and becomes very asymmetric, even in the undoped devices.

Thus, FWM shows a significant dependence on the temperature of the device but is a little more stable and less asymmetric in undoped QD SOAs.

Our FWM experiments yield important physical insight to the device dynamics, especially in the picosecond and subpicosecend regimes. If the FWM efficiency is plotted versus the frequency detuning (see Fig. 5) instead of the wavelength, distinct breakpoints can be observed, which are correlated to time constants. The first breakpoint is near 80 GHz, the second around 800 GHz and the third appears around 2 THz. From these frequencies three different time constants can be deduced. The first $\tau_1 = 1.9$ ps $\pm$ 0.2 ps for undoped SOAs (1.8 ps $\pm$ 0.2 ps for p-doped) can be attributed to the scattering time from the reservoir to the QDs, whereas $\tau_2 = 240$ fs $\pm$ 50 fs (220 fs $\pm$ 50 fs for p-doped) and $\tau_3 = 70$ fs $\pm$ 15 fs (80 fs $\pm$ 15 fs for p-doped) presumably present the intradot relaxation constants from ES to GS for electrons and holes, respectively. This is the first observation of two ultrafast time constants. Our results agree with the average time for the GS gain recovery known from pump probe measurements [5] and with the assumption in [26] that the hole GS and ES can be treated virtually as one state due to the ultrafast, almost instantaneous, carrier exchange between these states. Within the error margin, there is no difference between p-doped and undoped devices observable.

A slight decrease of the time constants with increasing carrier density is observed indicating that not only the competition between spectral hole burning on one hand and carrier heating and carrier density pulsation on the other hand changes, but also, the respective time constants become slightly faster. However, the temperature changes either accompanied by the increase of the operating current or by external heating cause no observable degradation of the time constants, in contrast to the FWM efficiency, which is strongly influenced by temperature effects.

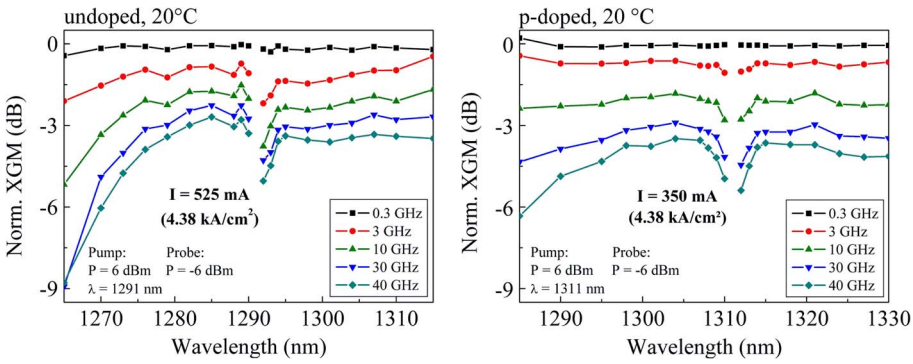

Fig. 6. (Left) Norm. XGM of the undoped QD SOAs is shown at certain frequencies dependent on the detuning. Between 1285 nm and 1292 nm, a XGM bandwidth beyond 40 GHz is achieved. (Right) Norm. XGM of the p-doped QD SOAs is shown at certain frequencies dependent on the detuning. The XGM bandwidth is limited to 25 to 30 GHz at same current density as on the left hand side.

5. Small-Signal XGM

In order to compare XGM of undoped and p-doped QD SOAs and to assess their suitability for wavelength conversion, small signal measurements were conducted. A strong pump signal saturates the SOA, changing the gain of the device. This gain change is scanned using a second nonsaturating probe signal at a different wavelength. If the saturating pump signal is modulated sinusoidally, the gain will also follow this modulation within the limits of the bandwidth given by the time constants of the gain material. Thus, the modulation of the pump signal is converted inversely to the probe signal.

The small-signal XGM is measured using a HP 8722C network analyzer (50 MHz to 40 GHz). The electrical S_{21}-parameter is converted to units of optical power. The traces are normalized to the pump response curve without amplification in the QD SOA to remove the responses of the modulator, electrical amplifiers, and the photo diode. Then, the XGM response is recorded as a function of detuning. For visualization values, five different frequencies between 300 MHz and 40 GHz are picked and plotted for the undoped and for the p-doped QD SOAs in Fig. 6.

The results are only shown for large current densities, because these enable the largest XGM bandwidths [8]. In general, the undoped devices tend to offer the largest bandwidth at a probe detuning to shorter wavelengths whereas the opposite is observed for the p-doped ones. This seems to be correlated with the wavelength position of the gain peak, as can be seen in Fig. 1, and indicates a strong coupling of the QDs to the reservoir and an indirect coupling of the subensembles mediated through the carrier reservoir in the QW at large current densities.

The absolute conversion efficiency defined as the ratio of the output probe modulation amplitude to the input pump modulation amplitude is comparable for both devices (-7 dB for the undoped and -8 dB for the p-doped QD SOAs) and almost independent of the temperature.

The undoped devices show a XGM bandwidth beyond our instrumental limit of 40 GHz between 1282 nm and 1289 nm at a current of 525 mA. For a small detuning, a dip in the XGM traces occurs near the pump wavelength, which is due to FWM.

The p-doped samples operated at the same current density are limited to 25 to 30 GHz and show a smaller bandwidth across the entire detuning range, except at the edges of the gain spectrum. Since p-doped samples are slightly more temperature stable it is possible, however, to drive them at larger current densities. In Fig. 7, XGM results measured at a current of 500 mA are presented corresponding to a current density 30% larger than the maximum for the undoped samples. Thus, also p-doped QD SOAs enable bandwidths beyond 40 GHz in the range of 1315 nm to 1330 nm.

These findings are consistent with the results presented in [14], where the dynamics of the p-doped QD SOAs were found to be slower. In [14], devices having the same length show slower gain recovery for p-doping, which are operated at lower current yielding the same gain for both

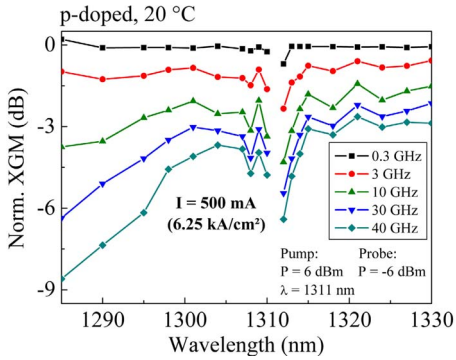

Fig. 7. Norm. XGM of the p-doped QD SOAs is shown at certain frequencies dependent on the detuning. At a current density of 6.25 kA /cm^2 (larger compared with Fig. 6) the bandwidth increases and is measured to be beyond 40 GHz near 1320 nm.

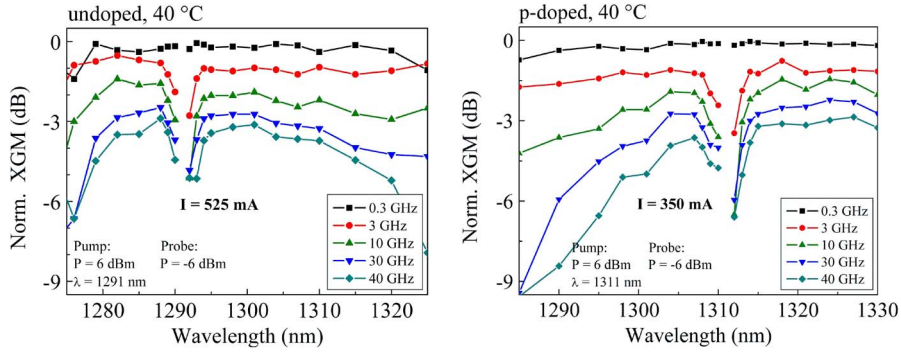

Fig. 8. (Left) Norm. XGM of the undoped QD SOAs is shown at certain frequencies dependent on the detuning for a device temperature of 40 °C. XGM bandwidths near 40 GHz are achieved. The bandwidths are comparable to the results taken at 20 °C. (Right) Norm. XGM of the p-doped QD SOAs is shown at certain frequencies dependent on the detuning for a device temperature of 40 °C. Due to suppressed NRR the XGM bandwidths are comparable to the undoped devices operated at the same current density.

devices. In this case, the reservoir in the ESs is only slightly populated, and the recovery is determined by the scattering time into the QDs being on the order of 1 to 10 ps, which is much slower than the intradot relaxation of 150 fs.

Additionally, the effective population is lower since the NRR processes consume a considerable amount of the carriers which, in turn, are not available for amplification. In combination with the larger gain this leads to a strongly reduced carrier reservoir population and a stronger coupling to the reservoir which has much slower carrier dynamics and, thus, limits the overall bandwidth.

For p-doped QD SOAs the NRR is suppressed at a temperature of 40 °C, as reported above. As a consequence, the XGM bandwidth and their dependence on the probe wavelength become comparable with the undoped devices at the same current density, because the effective current density, which is used to pump the QDs, is increased.

It is remarkable that the XGM bandwidth at 40 °C is for both devices still beyond 40 GHz (see Fig. 8), provided that high-frequency small-signal wavelength conversion is feasible within a temperature range of at least 20 °C to 40 °C without degrading bandwidth. Measurements at 60 °C were also conducted but showed low bandwidths between 10 to 15 GHz. This results from the lower saturation induced by the pump signal, since the gain shifts to longer wavelengths and decreases, leading to larger saturation input powers and, hence, less saturation.

In summary, it is necessary to operate the p-doped device at either a higher current density or at elevated temperatures to compensate for the NRR and to fill the reservoir in the ES sufficiently. Then, similar performance as with undoped QD SOAs is achieved.

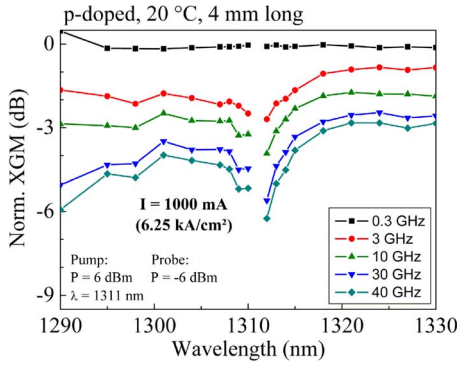

Fig. 9. Norm. XGM of p-doped 4-mm-long QD SOAs is shown at certain frequencies dependent on the detuning. This demonstrates that even with this long device 40-GHz XGM is feasible.

In comparison with our previous measurements [8], 40-GHz bandwidth is achieved only at a factor of two larger current densities. This is attributed to the changed waveguide design. The samples investigated here are shallow etched, whereas the samples investigated before were deeply etched through the active region, resulting in a larger confinement factor, less current spreading, and higher nonlinearity.

Finally, 4-mm-long p-doped QD SOAs were investigated in order to determine the influence of the length on the XGM bandwidth. In [27] and [28], it was observed that the longer the device is, the larger the XGM bandwidth becomes, if the devices are operated at the same current density. The 4-mm-long devices in [29] have a fiber-to-fiber gain of up to 26 dB. The chip gain is as large as 35 dB if the coupling losses of 4.5 dB per facet are considered. Making the devices even longer would result in considerable self-saturation by the ASE and therefore would not lead to a further increase of the gain. The 3-dB saturation output power in the fiber is 8 dBm, and the noise figure is below 10 dB. As depicted in Fig. 9, the XGM bandwidth is between 1318 nm and 1327 nm near 40 GHz. Although a bandwidth of nearly 40 GHz is achieved, no increase of the bandwidth, as predicted for QW SOAs, is found. In such a long device, the number of carriers consumed for amplification is so large that the carrier reservoir is strongly affected and depleted. Therefore, in these long devices, the saturation of the reservoir determines the overall bandwidth. Although the carrier lifetime in the reservoir is reduced and the bandwidth of the reservoir is increased, the influence of the QD dynamics is reduced. As a consequence, the XGM bandwidth is not larger in long QD SOAs.

6. Conclusion

P-doping has been shown to have two major influences on the performance of QD SOAs. First, the gain of the samples containing 10-fold-stacked QD layers is increased from 7 dB/mm to 10 dB/mm, which allows for shorter devices. On the other hand NRR is induced by the dopant. Thus, larger current densities are required to achieve the maximum linear gain. Temperature-dependent measurements reveal that the peak gain is achieved at lower current densities with increasing temperature. This results in the decreasing threshold current density of QD lasers. However, for QD SOAs, the peak gain is the figure of merit and this value decreases by 3 dB per 20 °C independent of the doping. In summary, p-doped QD SOAs are advantageous for linear amplification since shorter devices with lower noise figure can be fabricated to achieve a certain gain value.

The FWM measurements demonstrated decreased influence of carrier heating and carrier density pulsation in undoped QD SOAs due to the reduced coupling to the QW reservoir. This yields less asymmetry, better temperature stability, and larger chip-conversion efficiency of up to -2 dB.

In small-signal XGM experiments, a bandwidth of beyond 40 GHz was observed for the undoped devices, whereas the p-doped samples showed a bandwidth of 25 to 30 GHz at the same current density caused by the lower population of the reservoir and the NRR which lowers the effective

current density used for pumping the QDs. At larger current densities, the p-doped SOAs also achieve comparable bandwidths around or beyond 40 GHz.

For nonlinear applications, undoped QD SOAs should be preferred due to the fact that lower current densities are necessary for high-bandwidth operation.

Acknowledgment

The MBE growth of the wafers was done by Innolume GmbH, Dortmund, Germany. The authors are indebted to R. Molt and K. Janiak from the FhG Heinrich-Hertz-Institut, Berlin, Germany, for assistance with the AR-coating of the QD SOAs. They also want to thank Prof. Dr. A. Uskov for fruitful and in depth discussions.

References

[1] D. Bimberg, M. Kuntz, and M. Laemmlin, "Quantum dot photonic devices for lightwave communication," *Microelectron. J.*, vol. 36, no. 3–6, pp. 175–179, Mar.–Jun. 2005.
[2] D. Bimberg, M. Grundmann, and N. N. Ledentsov, *Quantum Dot Heterostructures*. Chichester, U.K.: Wiley, 1999.
[3] D. Bimberg, "Quantum dot based nanophotonics and nanoelectronics," *Electron. Lett.*, vol. 44, no. 3, pp. 168–170, Jan. 2008.
[4] D. Bimberg, M. Grundmann, N. N. Ledentsov, S. S. Ruvimov, P. Werner, U. Richter, J. Heydenreich, V. M. Ustinov, P. S. Kopev, and Z. I. Alferov, "Self-organization processes in MBE-grown quantum dot structures," *Thin Solid Films*, vol. 267, no. 1/2, pp. 32–36, Oct. 1995.
[5] P. Borri, W. Langbein, J. M. Hvam, F. Heinrichsdorff, H.-M. Mao, and D. Bimberg, "Spectral hole-burning and carrier-heating dynamics in InGaAs quantum-dot amplifiers," *IEEE J. Sel. Topics Quantum Electron.*, vol. 6, no. 3, pp. 544–552, May/Jun. 2000.
[6] A. V. Uskov, T. W. Berg, and J. Mork, "Theory of pulse-train amplification without patterning effects in quantum-dot semiconductor optical amplifiers," *IEEE J. Quantum Electron.*, vol. 40, no. 3, pp. 306–320, Mar. 2004.
[7] M. Sugawara, N. Hatori, M. Ishida, H. Ebe, Y. Arakawa, T. Akiyama, K. Otsubo, Y. Yamamoto, and Y. Nakata, "Recent progress in self-assembled quantum-dot optical devices for optical telecommunication: Temperature-insensitive 10 Gb s^{-1} directly modulated lasers and 40 Gb s^{-1} signal-regenerative amplifiers," *J. Phys. D, Appl. Phys.*, vol. 38, no. 13, pp. 2126–2134, Jun. 2005.
[8] C. Meuer, J. Kim, M. Laemmlin, S. Liebich, D. Bimberg, A. Capua, G. Eisenstein, R. Bonk, T. Vallaitis, J. Leuthold, A. R. Kovsh, and I. L. Krestnikov, "40 GHz small-signal cross-gain modulation in 1.3 μm quantum dot semiconductor optical amplifiers," *Appl. Phys. Lett.*, vol. 93, no. 5, p. 051110, Aug. 2008.
[9] T. Akiyama, M. Ekawa, M. Sugawara, K. Kawaguchi, H. Sudo, A. Kuramata, H. Ebe, and Y. Arakawa, "An ultrawide-band semiconductor optical amplifier having an extremely high penalty-free output power of 23 dBm achieved with quantum dots," *IEEE Photon. Technol. Lett.*, vol. 17, no. 8, pp. 1614–1616, Aug. 2005.
[10] S. Dommers, V. V. Temnov, U. Woggon, J. Gomis, J. Martinez-Pastor, M. Laemmlin, and D. Bimberg, "Complete ground state gain recovery after ultrashort double pulses in quantum dot based semiconductor optical amplifier," *Appl. Phys. Lett.*, vol. 90, no. 3, pp. 033508–033510, Jan. 2007.
[11] I. C. Sandall, P. M. Smowton, J. D. Thomson, T. Badcock, D. J. Mowbray, H. Y. Liu, and M. Hopkinson, "Temperature dependence of threshold current in p-doped quantum dot lasers," *Appl. Phys. Lett.*, vol. 89, no. 15, p. 151118, Oct. 2006.
[12] I. C. Sandall, P. M. Smowton, C. L. Walker, T. Badcock, D. J. Mowbray, H. Y. Liu, and M. Hopkinson, "The effect of p doping in InAs quantum dot lasers," *Appl. Phys. Lett.*, vol. 88, no. 11, p. 111113, Mar. 2006.
[13] D. G. Deppe, S. Freisem, H. Huang, and S. Lipson, "Electron transport due to inhomogeneous broadening and its potential impact on modulation speed in p-doped quantum dot lasers," *J. Phys. D, Appl. Phys.*, vol. 38, no. 13, pp. 2119–2125, Jun. 2005.
[14] V. Cesari, W. Langbein, P. Borri, M. Rossetti, A. Fiore, S. Mikhrin, I. Krestnikov, and A. Kovsh, "Ultrafast carrier dynamics in p-doped InAs/GaAs quantum-dot amplifiers," *IET Optoelectron.*, vol. 1, no. 6, pp. 298–302, Dec. 2007.
[15] V. Cesari, P. Borri, M. Rossetti, A. Fiore, and W. Langbein, "Refractive index dynamics and linewidth enhancement factor in p-doped InAs–GaAs quantum-dot amplifiers," *IEEE J. Quantum Electron.*, vol. 45, no. 6, pp. 579–585, Jun. 2009.
[16] T. Vallaitis, C. Koos, R. Bonk, W. Freude, M. Laemmlin, C. Meuer, D. Bimberg, and J. Leuthold, "Slow and fast dynamics of gain and phase in a quantum dot semiconductor optical amplifier," *Opt. Express*, vol. 16, no. 1, pp. 170–178, Jan. 2008.
[17] D. G. Deppe, H. Huang, and O. B. Shchekin, "Modulation characteristics of quantum-dot lasers: The influence of p-type doping and the electronic density of states on obtaining high speed," *IEEE J. Quantum Electron.*, vol. 38, no. 12, pp. 1587–1593, Dec. 2002.
[18] I. C. Sandall, P. M. Smowton, C. L. Walker, H. Y. Liu, M. Hopkinson, and D. J. Mowbray, "Recombination mechanisms in 1.3 μm InAs quantum-dot lasers," *IEEE Photon. Technol. Lett.*, vol. 18, no. 8, pp. 965–967, Apr. 2006.
[19] C. Meuer, J. Kim, M. Laemmlin, S. Liebich, A. Capua, G. Eisenstein, A. R. Kovsh, S. S. Mikhrin, I. L. Krestnikov, and D. Bimberg, "Static gain saturation in quantum dot semiconductor optical amplifiers," *Opt. Express*, vol. 16, no. 11, pp. 8269–8279, May 2008.
[20] A. V. Uskov, E. P. O'Reilly, M. Laemmlin, N. N. Ledentsov, and D. Bimberg, "On gain saturation in quantum dot semiconductor optical amplifiers," *Opt. Commun.*, vol. 248, no. 1–3, pp. 211–219, Apr. 2005.

[21] J. Kim, M. Laemmlin, C. Meuer, D. Bimberg, and G. Eisenstein, "Theoretical and experimental study of high-speed small-signal cross-gain modulation of quantum-dot semiconductor optical amplifiers," *IEEE J. Quantum Electron.*, vol. 45, no. 3, pp. 240–248, Mar. 2009.
[22] D. Bimberg, C. Meuer, M. Lammlin, S. Liebich, J. Kim, A. Kovsh, I. Krestnikov, and G. Eisenstein, "Nonlinear properties of quantum dot semiconductor optical amplifiers at 1.3 μm," *Chin. Opt. Lett.*, vol. 6, no. 10, pp. 724–726, 2008.
[23] D. Nielsen, S. L. Chuang, N. J. Kim, D. Lee, S. H. Pyun, W. G. Jeong, C. Y. Chen, and T. S. Lay, "High-speed wavelength conversion in quantum dot and quantum well semiconductor optical amplifiers," *Appl. Phys. Lett.*, vol. 92, no. 21, p. 211101, May 2008.
[24] T. Akiyama, H. Kuwatsuka, N. Hatori, Y. Nakata, H. Ebe, and M. Sugawara, "Symmetric highly efficient ($\sim$0 dB) wavelength conversion based on four-wave mixing in quantum dot optical amplifiers," *IEEE Photon. Technol. Lett.*, vol. 14, no. 8, pp. 1139–1141, Aug. 2002.
[25] A. Bilenca, R. Alizon, V. Mikhelashvili, D. Dahan, G. Eisenstein, R. Schwertberger, D. Gold, J. P. Reithmaier, and A. Forchel, "Broad-band wavelength conversion based on cross-gain modulation and four-wave mixing in InAs–InP quantum-dash semiconductor optical amplifiers operating at 1550 nm," *IEEE Photon. Technol. Lett.*, vol. 15, no. 4, pp. 563–565, Apr. 2003.
[26] T. Piwonski, I. O'Driscoll, J. Houlihan, G. Huyet, R. J. Manning, and B. Corbett, "Gain and phase dynamics of InAs/GaAs quantum dot semiconductor optical amplifiers," in *Proc. 10th Anniversary Int. Conf. Transparent Opt. Netw.*, 2008, vol. 2, pp. 145–148, 212.
[27] T. Durhuus, B. Mikkelsen, C. Joergensen, S. L. Danielsen, and K. E. Stubkjaer, "All-optical wavelength conversion by semiconductor optical amplifiers," *J. Lightwave Technol.*, vol. 14, no. 6, pp. 942–954, Jun. 1996.
[28] C. Joergensen, S. L. Danielsen, K. E. Stubkjaer, M. Schilling, K. Daub, P. Doussiere, F. Pommerau, P. B. Hansen, H. N. Poulsen, A. Kloch, M. Vaa, B. Mikkelsen, E. Lach, G. Laube, W. Idler, and K. Wunstel, "All-optical wavelength conversion at bit rates above 10 Gb/s using semiconductor optical amplifiers," *IEEE J. Sel. Topics Quantum Electron.*, vol. 3, no. 5, pp. 1168–1180, Oct. 1997.
[29] G. Fiol, C. Meuer, H. Schmeckebier, D. Arsenijevic, S. Liebich, M. Laemmlin, M. Kuntz, and D. Bimberg, "Quantum-dot semiconductor mode-locked lasers and amplifiers at 40 GHz," *IEEE J. Quantum Electron.*, vol. 45, no. 11, pp. 1429–1435, Nov. 2009.